Nonlinear optical behaviors in a silver nanoparticle array at different wavelengths*

Yu Ben-Hai(余本海),† Zhang Dong-Ling(张东玲), Li Ying-Bin(李盈傧), and Tang Qing-Bin(汤清彬)

College of Physics and Electronic Engineering, Xinyang Normal University, Xinyang 464000, *China*

(Received 8 April 2012; revised manuscript received 19 June 2012)

The optical nonlinearities of an Ag nanoparticle array are investigated by performing Z-scan measurements at the selected wavelengths (400, 600, 650, and 800 nm). The nonlinear refraction index in the resonant region (around 400 nm) exhibits a significant enhancement by two orders compared with that in the off-resonant region (around 800 nm)), and exhibits an sign alternation of the resonant nonlinear absorption, which results in a negligible nonlinear absorption at a certain excitation intensity. Moreover, a low degree of nonlinear absorption was measured at the edges of the resonant region (600 and 650 nm), which is attributed to the competition of the saturated absorption and the two-photon absorption processes.

Keywords: third-order optical nonlinearity, Ag nanoparticles, nanosphere lithography

PACS: 42.70.Nq, 78.67.Bf, 81.16.Nd **DOI:** 10.1088/1674-1056/22/1/014212

1. Introduction

Due to large nonlinear optical effects and fast response time, the nonlinear optical properties of noble metal nanoparticles have been investigated actively.[1–11] In particular, silver nanoparticles have a strong surface plasmon resonance (SPR) absorption in the ultraviolet–visible (UV–Vis) region, which opens many potential applications, such as optical limiting[1,2] and all-optical switching.[3,5] For a Mach–Zehnder-based switch, the required phase shift $\triangle\phi = \pi$ has driven people to search for a nonlinear material with large nonlinear refraction (NLR) and small linear and nonlinear absorption (NLA). One- ($W = (|n_2|I_s)/(\alpha_0\lambda)$) and two-photon ($T = (\alpha_2\lambda/|n_2|)$) figures of merit (FOM) are used to evaluate the quality of the nonlinear optical materials, where I_s is the saturation intensity at which the change in the nonlinear refractive index saturates, α_0 is the linear absorption coefficient, α_2 is the NLA coefficient, n_2 is the NLR index, and λ is the central wavelength. A suitable candidate for all-optical switching requires $W \gg 1$ and $T \ll 1$.[3,12]

Due to the strong optical enhancement in the resonant region, the resonant optical nonlinearities of noble nanoparticles have been extensively investigated.[8–11] However, strong NLA can lead to great loss, which greatly limits the applications of noble metals. In order to avoid linear and nonlinear losses, many studies are focused on the off-resonant nonlinear properties of noble metal nanoparticles.[13–15] However, a small NLR index (down to 10^{-3} cm^2/GW) and a high pump intensity (up to 100 GW/cm^2) limit the application in all-optical switching. Since the optical nonlinearities are quite different in the off-resonant and resonant regions, it is important to understand different nonlinear response mechanisms in different regions. However, to the best of our knowledge, the study of the optical nonlinearities in Ag nanoparticles in a broadband (400–800 nm) is absent.

In this paper, nonlinearities of an Ag periodical particle array (PPA) at resonant (400 nm), off-resonant (800 nm), and the edge of resonant regions (600 and 650 nm) are investigated. The large enhancement of the NLR effect in the resonant region is obtained. As the excitation intensity increases, a reversal of the sign of the NLA coefficient in the resonant region is observed clearly in experiments, indicating that the NLA can be neglected at a certain excitation intensity (I_s). Two FOMs (i.e., $W = 3$ and $T \sim 0$) are obtained at a low excitation intensity of 12 GW/cm^2 in the resonant region, which is much lower than that in the off-resonant region (150 GW/cm^2). Moreover, due to the competition of saturated absorption (SA) and two-photon absorption (TPA) processes, a low NLA effect was measured at the edges of the resonant region.

2. Experiment procedure

The Ag PPA was fabricated using the nanosphere lithography (NSL) method.[16] The diameter of the polystyrene nanosphere was 300 ± 5 nm. In the PLD processing step, a KrF (Lambda Physik, 248 nm) laser was used as the laser source, the energy density focused on the target was about 2 J/cm^2, and the repetition frequency was 6 Hz. The deposition time was set to be 30 min. The sample was annealed

*Project supported by the National Natural Science Foundation of China (Grant Nos. 11005088 and 11047145), the Science and Technology Project of Henan Province, China (Grant Nos. 102300410241 and 112300410021), and the Scientific Research Foundation of Education Department of Henan Province, China (Grant No. 2011B140018).

†Corresponding author. E-mail: hnyubenhai@163.com

© 2013 Chinese Physical Society and IOP Publishing Ltd

at a low temperature of 150 °C for an hour. The morphology of the Ag particles was observed by SEM (FEI QUANTA 200), which shows an area as large as 100–1000 μm^2. The inset in Fig. 1 clearly shows the shape and the size of the Ag particles with rounded tips. The in-plane perpendicular bisector is $a = 60$ nm, and the out-of-plane particle height is $b = 20$ nm. The SPR spectrum was measured with UV–Vis absorption spectroscopy (U-3310 UV solutions) in a wavelength range of 200–900 nm.

The nonlinear optical properties were determined by using the Z-scan method, which is well described elsewhere.[17] In Z-scan experiments, we employ laser pulses from an optical parametric amplifier (TOPAS, light conversion) pumped by 50-fs pulses at 800 nm, and delivered by a mode-locked Ti: Sapphire oscillator as well as a regenerative amplifier (Spitfire, Spectra-Physics) operating at a 1 kHz repetition rate. The 400-nm pulses were produced in a β-barium borate crystal (BBO) pumped by a 800-nm femtosecond Ti: sapphire laser. The sample was scanned along the optical axis (the z direction) and focused by a lens with a focal length of 200 mm. For different wavelengths, the radius of the beam waist (ω_0) ranged from 21 to 30 μm. The value of the Rayleigh length ($z_0 = \pi\omega_0^2/\lambda$) was calculated to be 3.5 mm, which is much greater than the thickness either of the substrate (0.2 mm) or the sample. The damage threshold was measured to be 850 GW/cm^2 in the off-resonant region and 60 GW/cm^2 in the resonant region.

3. Results and discussion

Due to the high uniformity of Ag nanoparticles as shown in the inset of Fig. 1, a strong SPR peak located at 400 nm is observed. The linear absorption coefficients at 400, 600, and 650 nm ($\alpha_0^{400\ \mathrm{nm}}$, $\alpha_0^{600\ \mathrm{nm}}$, and $\alpha_0^{650\ \mathrm{nm}}$) are estimated to be 10, 2, and 1.1 times $\alpha_0^{800\ \mathrm{nm}}$, respectively. The Ag PPA in our experiment can be considered as a Maxwell–Garnet geometry that is the ordered Ag nanoparticles embedded in air matrices. The effective dielectric constant of composite material is given by[18,19]

$$\varepsilon_{\mathrm{eff}} = \varepsilon_{\mathrm{h}}\left(\frac{1+2\beta p}{1-\beta p}\right), \tag{1}$$

where $\beta = (\varepsilon_{\mathrm{i}} - \varepsilon_{\mathrm{h}})/(\varepsilon_{\mathrm{i}} + 2\varepsilon_{\mathrm{h}})$, $\varepsilon_{\mathrm{h}} = 1$ is the dielectric constant of the host material for air matrices, and ε_{i} is the dielectric constant of the Ag nanoparticle. Since the metal volume fraction p is low ($p = 0.08$), equation (1) can be simplified into[20]

$$\varepsilon_{\mathrm{eff}} = \varepsilon_{\mathrm{h}} + 3\varepsilon_{\mathrm{h}} p\left(\frac{\varepsilon_{\mathrm{i}} - \varepsilon_{\mathrm{h}}}{\varepsilon_{\mathrm{i}} + 2\varepsilon_{\mathrm{h}}}\right). \tag{2}$$

For ultrashort pulses, the relationship of the contribution of the hot electron ($\chi_{\mathrm{m}}^{(3)}$) with the corresponding susceptibility response to the local field E_{loc} and $\chi_{\mathrm{eff}}^{(3)}$ are given by

$$\chi_{\mathrm{eff}}^{(3)} = p f^2 |f|^2 \chi_{\mathrm{m}}^{(3)}, \tag{3}$$

where f is the ratio between the local field E_{loc} and the applied field E_0, and

$$E_{\mathrm{loc}} = fE_0 = \frac{3\varepsilon_{\mathrm{h}}}{\varepsilon_{\mathrm{i}} + 2\varepsilon_{\mathrm{h}}} E_0. \tag{4}$$

In the large particle limit, it is appropriate to calculate ε_{i} from the data for bulk Ag.[21] Thus, the local-field factor at 400, 600, and 650 nm ($f_{400\ \mathrm{nm}}$, $f_{600\ \mathrm{nm}}$, and $f_{650\ \mathrm{nm}}$) are estimated to be 8.6, 1.95, and 1.62 times of $f_{800\ \mathrm{nm}} = 0.11$, respectively.

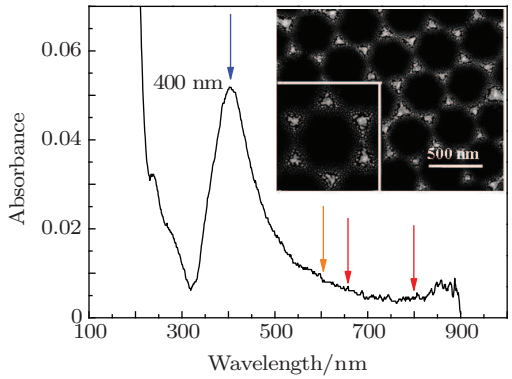


Fig. 1. (color online) Absorption spectrum of an Ag nanoparticle array with an SPR peak at 400 nm. The arrows indicate the wavelengths of the excitation laser (400, 600, 650, and 800 nm).

Figure 2(a) shows typical closed-aperture (CA) Z-scan data of the Ag PPA in the off-resonant region (800 nm) under different excitation intensities at the focal point (I_0) of 55, 125, 210, and 280 GW/cm^2. The CA Z-scan data of the Ag PPA exhibit valley/peak curves, indicating a positive NLR index due to self-focusing. The asymmetric curves are attributed to the influence of the NLA effect: the peak is suppressed at a low excitation intensity ($I_0 = 55$ GW/cm^2), which implies a positive NLA index due to the TPA effect. As the excitation intensity increases to 125 GW/cm^2, the appearance of a symmetric curve indicates the decrease of the NLA coefficient. As the intensity further increases, the curves show an enhanced peak and suppressed valley, implying a negative NLA value and a dominate role of the SA process. To quantify these nonlinear processes, the normalized transmittance is given by[22]

$$T = 1 + \frac{2(-\rho x^2 + 2x - 3\rho)}{(x^2+9)(x^2+1)}\Delta\Phi, \tag{5}$$

where $\rho = \alpha_2/(2kn_2)$ is the ratio of the NLA to the NLR, and $\Delta\Phi = kn_2 I_0 L_{\mathrm{eff}}$ is the phase shift due to the NLR. Both the NLA and NLR results can be obtained by fitting the CA curves with this model.

The open-aperture (OA) curves in Fig. 2(b) clearly show the process of the reversal of the NLA sign, which is in accordance with the results of the CA curves. As the excitation intensity increases, the NLA processes change from TPA to SA. Due to the strong absorption at 400 nm, the TPA process plays a dominate role when the intensity is relatively low (55 GW/cm^2). As the intensity increases (125 and

210 GW/cm^2), a transition process from TPA to SA occurs. The SA process becomes dominant as the intensity further increases (280 GW/cm^2). The intensity threshold is estimated to be 150 GW/cm^2, at which the NLA can be neglected.

Figures 3(a) and 3(b) show the CA and OA Z-scan data of the Ag PPA in the resonant region (400 nm) under different excitation intensities of 4, 12, 20, and 25 GW/cm^2. In Fig. 3(a), the CA curves exhibit a sign alternation of the NLR, which shows a different nonlinear response from the processes shown in Fig. 2(a). At a low excitation intensity (4 GW/cm^2), an enhanced peak and a suppressed valley appear on these curves, which implies a negative NLR index sign and an NLA component due to the SA effect. At a moderate intensity (12 GW/cm^2), there exist a flat OA curve and a standard peak/valley curve. At a higher intensity of 25 GW/cm^2, we observe valley/peak curves, indicating a positive sign of the NLR index due to self-focusing, while the enhanced valley and suppressed peak indicate a positive NLA component due to the reverse saturated absorption (RSA) effect. The curve with an intensity of 20 GW/cm^2 shows two peaks as well as a valley around the focal point on the Z axis, indicating a transition process from self-defocusing to self-focusing. It clearly shows that a large NLR index and a negligible NLA can be obtained at a low intensity of 12 GW/cm^2.

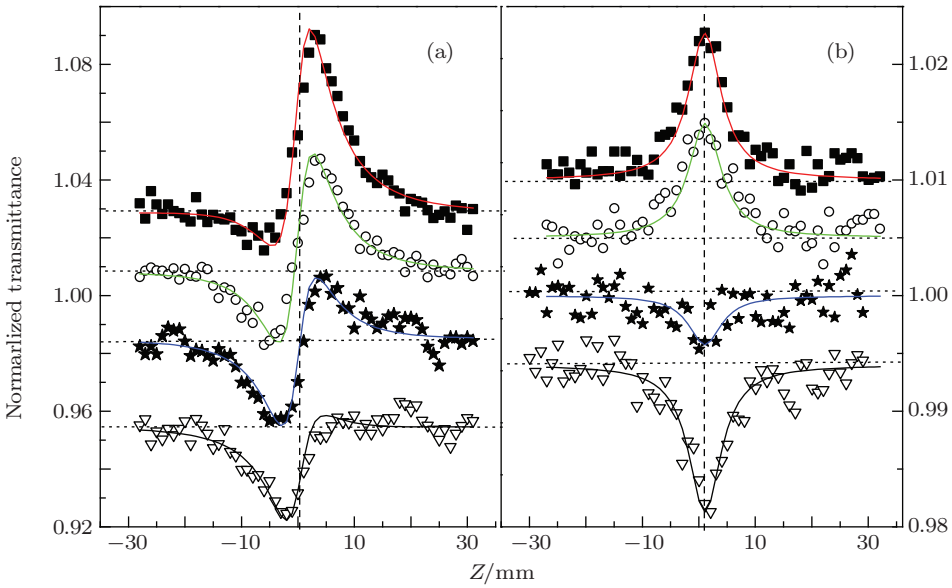


Fig. 2. (color online) (a) CA and (b) OA Z-scan results in an off-resonant region (800 nm) at different excitation intensities with the focal point $I_0 = 55$ (triangles), 125 (stars), 210 (circles), and 280 GW/cm^2 (squares). The solid lines denote the theoretical fitting.

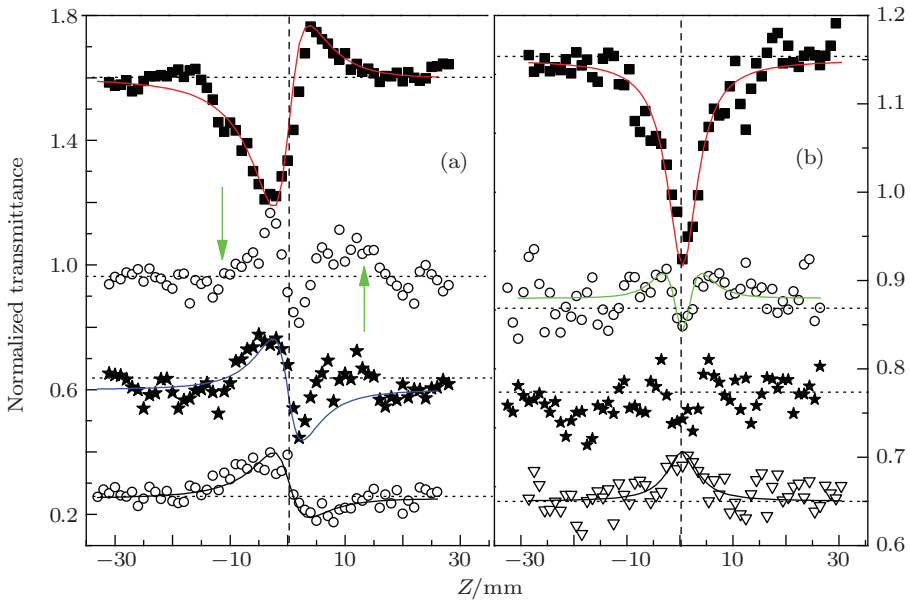


Fig. 3. (color online) (a) CA and (b) OA Z-scan results in the resonant region (400 nm) at different excitation intensities with the focal point $I_0 = 4$ (triangles), 12 (stars), 20 (circles), and 25 GW/cm^2 (squares). The solid lines denote the theoretical fitting.

The nonlinear process of the reversal of the NLA sign can also be clearly observed from the OA curves, as shown in Fig. 3(b). As the excitation intensities increase, the NLA processes change from SA to RSA, which is in agreement with the results shown in Fig. 3(a). The SA process attributed to the ground-state bleaching plays a dominant role at the low intensity, and the RSA process becomes important as the intensity increases.

The plasmon band of noble metal nanoparticles involves oscillations of the conduction electron in response to a laser pulse. The absorption of the plasmon band is highly sensitive to the wavelength of the excitation laser pulse. The absorption coefficient in the SPR region increases by 10 times compared with that in the off-resonant region (see Fig. 1). In the case of 800 nm (see Fig. 2), even if 2ω is smaller than the interband transition threshold, the TPA effect is still observed under a relatively low intensity of 55 GW/cm^2. This is due to a negligible $\alpha_0^{800\ \mathrm{nm}}$ with a significant absorption for 2ω (400 nm) matching the SPR region. As the intensity increases, the ground-state beaching of the conduction electron occurs, leading to the SA effect. At a high intensity of 280 GW/cm^2, the SA process is dominated.

In the cases of 600 and 650 nm, a low nonlinear absorption is observed even under high intensities. Since the energy of 2ω matches the intensity threshold (4 eV, 310 nm), the interband transition process due to the TPA process becomes comparable to the SA process due to the ground-state bleaching effect even under high intensities. Since 2ω is close to the bottom of the plasmon band (about 620 nm) theoretically, these two mechanisms cancel each other out, resulting in a low nonlinear absorption in the region. A similar phenomenon has been observed in other material systems, such as a MEH–PPV/chloroform solution and a ZnO film.[24,25] However, the large interband transition threshold makes the one-photon interband transition impossible for the Ag nanoparticle in the visible region, and the SA process is attributed to the ground-state bleaching of the conduction electron.

In the resonant region of 400 nm, the absorption of the plasmon band increases significantly, resulting in an SA process even under a low intensity of 4 GW/cm^2. As the intensity increases, the contribution from the free-carrier absorption becomes important, which results in the RSA process. Additionally, the two-photon electron ejection occurs due to the energetic photons at a wavelength of 400 nm, which can also lead to the RSA process. A similar mechanism transition (from SA to RSA) in the Ag nanoparticles is observed at a wavelength of 532 nm.[9]

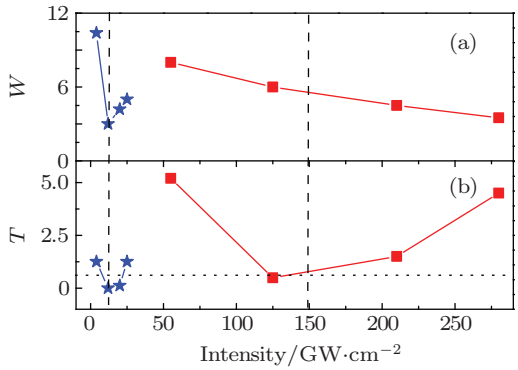


Fig. 4. (color online) (a) One- and (b) two-photon FOMs of the Ag nanoparticles as a function of intensity at wavelengths of 400 (stars) and 800 nm (squares).

By comparing the fitted results of the Ag PPA in Table 1, the $n_2^{400\ \mathrm{nm}}$ is calculated to be 0.36 cm^2/GW, which shows an enhancement by two orders compared with $n_2^{800\ nm}$ (4.8×10^{-3} cm^2/GW) in the off-resonant region due to the strong SPR enhancement effect. Because of the sign alternation of NLA, α_2 can be neglected in an excitation intensity. As shown in Fig. 4, $I_s^{400\ \mathrm{nm}}$ and $I_s^{800\ \mathrm{nm}}$ are estimated to be 12 and 150 GW/cm^2, respectively. At an intensity of 12 GW/cm^2 and wavelength of 400 nm, the FOMs $W = 3$ and $T \sim 0$ are obtained.

Table 1. Fitted results of optical nonlinearities of the Ag PPA at different wavelengths.

I_0 /GW·cm^{-2}	$\alpha_2^{400\ \mathrm{nm}}$ /cm·GW^{-1}	$n_2^{400\ \mathrm{nm}}$ /cm^2·GW^{-1}	$\alpha_2^{800\ \mathrm{nm}}$ /cm·GW^{-1}	$n_2^{800\ \mathrm{nm}}$ /cm^2·GW^{-1}	$\alpha_2^{600\ \mathrm{nm}}$ /cm·GW^{-1}	$\alpha_2^{650\ \mathrm{nm}}$ /cm·GW^{-1}
4	-3.8×10^4	–0.9	–	–	–	–
12	~0	–0.26	–	–	–	–
20	1.1×10^3	0.36	–	–	–	–
25	1.2×10^4	0.37	–	–	–	~0
55	–	–	5.5×10^2	8.5×10^{-3}	~0	~0
125	–	–	40	6.5×10^{-3}	~0	75
210	–	–	–90	4.8×10^{-3}	~0	70
280	–	–	-2.1×10^2	3.7×10^{-3}	~0	50

4. Conclusion

In summary, a tip-rounded Ag PPA was fabricated with the NSL method. The wavelength-related nonlinear optical properties were investigated by a Z scan using a femtosecond laser at different excitation intensities (400, 600, 650, and 800 nm). In the resonant region, a strong enhancement of the nonlinear refraction index was observed and the nonlinear absorption can be neglected due to the sign alternation at a low excitation intensity of 12 GW/cm^2. The FOMs of an Ag PPA at 400 nm, $W = 3$ and $T \sim 0$, are obtained, indicating low linear and nonlinear losses. A low nonlinear response at the edges of the resonant region was also observed.

References

[1] Seo J T, Yang Q G, Kim W J, Heo J H, Ma S M, Austin J, Yun W S, Jung S S, Han S W, Tabibi B and Temple D 2009 *Opt. Lett.* **34** 307

[2] Wang K, Zhou J, Yuan L Y, Tao Y T, Chen J, Lu P X and Wang Z L 2012 *Nano Lett.* **12** 833

[3] Wang Q Q, Han J B, Gong H M, Chen D J, Zhao X J, Feng J Y and Ren J J 2006 *Adv. Func. Mat.* **16** 2405

[4] Fan G H, Qu S L, Guo Z Y, Wang Q and Li Z G 2012 *Chin. Phys.* B **21** 047804

[5] Inouye H, Tanaka K, Tanahashi I, Hattori T and Nakatsuka H 2000 *Jpn. J. Appl. Phys.* **39** 5132

[6] Zhou H C, Yang G, Wang K, Long H and Lu P X 2010 *Opt. Lett.* **35** 4112

[7] Wang K, Long H, Fu M, Yang G and Lu P X 2010 *Opt. Express* **18** 13874

[8] Jayabalan J, Singh A, Charl R and Oak S M 2007 *Nanotechnology* **18** 315704

[9] Gurudas U, Brooks E, Bubb D M, Heiroth S, Lippert T and Wokaun A 2008 *J. Appl. Phys.* **104** 073107

[10] Fu M, Long H, Wang K, Yang G and Lu P X 2011 *Thin Solid Films* **519** 6557

[11] Long H, Chen A P, Yang G, Li Y H and Lu P X 2009 *Thin Solid Films* **517** 5601

[12] Fu M, Wang K, Long H, Yang G, Lu P X, Hetsch F, Susha A S and Rogach A L 2012 *Appl. Phys. Lett.* **100** 063117

[13] Unnikrishnan K P, Nampoori V P N, Ramakrishnan V, Umadevi M and Vallabhan C P G 2003 *J. Phys.* D **36** 1242

[14] Li T, Yu L, Lu Z X, Song G and Zhang K 2011 *Chin. Phys.* B **20** 087805

[15] Wang K, Long H, Fu M, Yang G and Lu P X 2010 *Opt. Lett.* **35** 1560

[16] Huang W Y, Qian W and El-Sayed M A 2005 *J. Phys. Chem.* B **109** 18881

[17] Sheik-Bahae M, Said A A, Wei T H, Hagan D J and Van Stryland E W 1990 *IEEE J. Quantum Electron.* **26** 760

[18] Boyd R W, Gehr R J, Fischer G L and Sipe J E 1996 *Pure Appl. Opt.* **5** 505

[19] Sipe J E and Boyd R W 1992 *Phys. Rev.* A **46** 1614

[20] Ricard D, Roussignol Ph and Flytzanis Chr 1985 *Opt. Lett.* **10** 511

[21] Lide D R 2001 *Handbook of Chemistry and Physics* (Florida: CRC)

[22] Liu X D, Guo S L, Wang H T and Hou L T 2001 *Opt. Commun.* **197** 431

[23] Kaplan A E and Volkov S N 2008 *Phys. Rev. Lett.* **101** 133902

[24] De Boni L, Andrade A A, Corrča D S, Balogh D T, Zilio S C, Misoguti L and Mendonca C R 2004 *J. Phys. Chem.* B **108** 5221

[25] Vivas M G, Shih T, Voss T, Mazur E and Mendonca C R 2010 *Opt. Express* **18** 9628